JOURNAL OF SPACECRAFT AND ROCKETS
Vol. 37, No. 4, July–August 2000

Relative Heat Load Comparison of Vehicles Flying Hypersonic Transatmospheric Trajectories

Falcon Rankins* and Darryll J. Pines†
University of Maryland, College Park, Maryland 20742

An approximate analysis to estimate the stagnation-point heat flux and heat load for hypersonic vehicles flying transatmospheric periodic, glide, and steady-state cruise trajectories is presented. The analysis was developed by approximating density and velocity profiles for a hypersonic vehicle with aerodynamic characteristics that are assumed to be representative of current and future configurations. Results from a comparative investigation of relative heating rates and heating loads suggest that there exists a flight corridor of mean altitudes and cruise velocities at which a periodic cruise trajectory achieves lower average heating rates when compared to glide or steady-state cruise trajectories.

Nomenclature

C_D = drag coefficient
C_L = lift coefficient
D = drag, N
g_w = ratio of wall enthalpy to total enthalpy
L = lift, N
m = vehicle mass, kg
q = heat load, J/cm^2
$\dot{q}$ = heat flux, W/cm^2
R = trajectory range, m
r_n = body nose radius, m
r_0 = radius of the Earth, m
t = time, s
V = vehicle velocity, m/s
V_{boost} = glide trajectory starting velocity, m/s
V_s = orbital velocity at surface of Earth, m/s
x = horizontal distance along path, m
y = altitude, m
y_a = maximum periodic trajectory amplitude, m
y_c = mean altitude of a periodic trajectory, m
y_f = ending altitude of glide trajectory, m
y_i = starting altitude of glide trajectory, m
β = density profile scale factor, m^{-1}
γ = flight-path angle, rad
γ_f = flight-path angle at periodic hypersonic cruise (PHC) mean altitude, rad
ρ = density, kg/m^3
ρ_0 = reference density, kg/m^3
ω = periodic trajectory frequency, rad/m

Subscripts

glide = glide trajectory
phc = PHC trajectory
ss = steady state
steady = steady-state cruise trajectory

Introduction

In the past four decades there has been considerable interest in developing hypersonic vehicles for a variety of applications. Recent interest in hypersonic flight has been motivated by the potential for long-range intercontinental transport involving both cargo and passengers with the shortest possible travel times. These efforts have focused on hypersonic vehicle designs, which can deliver the maximum amount of payload for a given range. To achieve this goal, various flight trajectories have been studied, including steady-state hypersonic cruise, boost-glide, and periodic cruise. Of these trajectory types, optimal periodic cruise trajectories appear to be the most promising in terms of average fuel consumption for a given range.

Following the lead of Speyer[1,2] and more recent studies by Chuang and Morimoto,[3] Carter et al.[4] and vE. Rudd et al.[5] analyzed optimal periodic hypersonic cruise (PHC) trajectories for increased performance. PHC trajectories use a skipping motion with periodic propulsion impulses at the lowest altitude of the trajectory to sustain the skipping motion. An example of a PHC trajectory can be seen in Fig. 1. Both initial approximate analyses and more rigorous optimization studies suggest that PHC trajectories provide better performance than other trajectory types. Although previous work[3,5] considered heating issues as a constraint in trajectory design, the work neglected to address adequately the issue of the heat flux and heat load encountered by a hypersonic vehicle traveling along a PHC trajectory path.

Thus, a simple analytical method of estimating the heat flux and heat load experienced on a PHC trajectory is desired. Although analytical entry heating analyses have been treated in some detail,[6–8] little work has been done toward an analytical heating analysis of a periodic trajectory. The present work attempts to develop the necessary analytical tools for estimating the stagnation-point heat flux and integrated heat load on a vehicle flying a PHC trajectory. This analysis is compared to similar analyses for hypersonic steady-state cruise and glide trajectories in an attempt to compare the trajectory types.

Simplified Heating Analysis

Trajectory Approximations

In the subsequent simplified heating analysis, the following assumptions are applied to each trajectory type: 1) boost phase is ignored, 2) atmosphere is exponential, 3) g forces are acceptable from a structural standpoint, 4) vehicle mass remains constant, and 5) vehicle lift-to-drag ratio is held constant.

PHC Trajectory

The altitude profile for a PHC trajectory can be approximated by

$$y = y_c + y_a \cos \omega x \tag{1}$$

where ω is defined in terms of range as $2\pi/R$, where R is the straight-line distance between the endpoints of a single period. At any point along the trajectory, the flight-path angle is γ, and the absolute value of the flight-path angle at the mean altitude of the trajectory is γ_f.

Received 13 August 1999; revision received 18 February 2000; accepted for publication 18 March 2000.

*Undergraduate Researcher, Department of Aerospace Engineering. Student Member AIAA.
†Assistant Professor, Department of Aerospace Engineering. Senior Member AIAA.

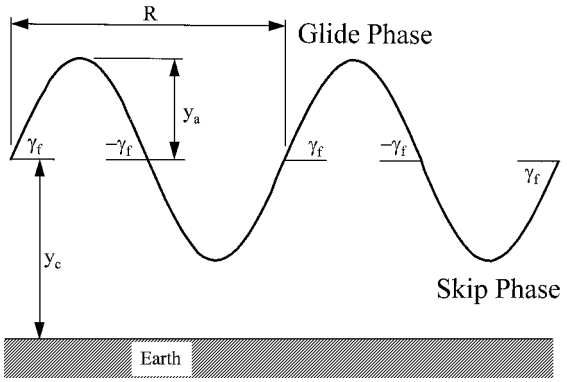

Fig. 1 Parameters of a PHC trajectory.

Definition of Steady-State Cruise Trajectory

The hypersonic steady-state cruise trajectory is approximated by a straight and level path. It is flown at a constant velocity V_{ss} and steady-state altitude y_{ss}.

Definition of Hypersonic Glide Trajectory

For the purposes of this analysis, the glide trajectory is approximated as a linear path connecting designated starting and ending points. The starting point of the trajectory is significantly higher than the mean altitude of either a typical periodic or steady-state cruise trajectory. The glide trajectory can then be written as

$$y_{\text{glide}}(x) = \frac{y_f - y_i}{R_{\text{glide}}} x + y_i \tag{2}$$

Heat Flux Equation

From Tauber et al.[7] the stagnation-point heating rate can be written as

$$\dot{q} = \frac{\mathrm{d}q}{\mathrm{d}t} = C\rho^{\frac{1}{2}} V^3 \tag{3}$$

such that

$$C = 1.83(10^{-8}) r_n^{-\frac{1}{2}} (1 - g_w) \tag{4}$$

where the ratio of wall enthalpy to total enthalpy g_w is a weak function of wall temperature. If the velocity is entered in meters per second and the density in kilograms per cubic meter, the resulting units of heat flux are watts per square centimeter.

Because the various trajectory types will be defined with respect to distance rather than time, the heating rate must be rewritten in terms of distance. It can easily be seen that for a given point along a periodic trajectory

$$\frac{\mathrm{d}x}{\mathrm{d}t} = V \cos\gamma \tag{5}$$

where γ is the flight-path angle at a given trajectory point.

Combining Eq. (3) with Eq. (5) describes the change in heat load over distance x:

$$\frac{\mathrm{d}q}{\mathrm{d}x} = \frac{C\rho^{\frac{1}{2}} V^2}{\cos\gamma} \tag{6}$$

Density Profile

To use the equation effectively for heating rate, a density profile along the trajectory is required. The density profile can be approximated by assuming the exponential atmospheric model given by Nørstrud[8]:

$$\rho = \rho_0 e^{-\beta y} \tag{7}$$

where ρ_0 is the sea level density of 1.225 kg/m^3 and the density scaling factor β is 0.00014 m^{-1}. This density function provides values corresponding to standard atmosphere density values at altitudes of 0, 30.2, and 54 km. Between the altitudes of 30 and 54 km, the exponential approximation to the atmosphere slightly overestimates the density.

Heating Analysis for PHC

Stagnation Heat Flux with Constant Velocity

Combining Eq. (1) with Eq. (7) provides the density variation encountered along a periodic trajectory as a function of distance along the trajectory:

$$\rho = \rho_0 \exp[-\beta(y_c + y_a \cos\omega x)] \tag{8}$$

To simplify matters, the heating analysis is initially performed with the assumption that velocity remains a constant, V_0, along the trajectory. The heating equation then becomes

$$\frac{\mathrm{d}q_{\text{phc}}}{\mathrm{d}x} = C\frac{V_0^2}{\cos\gamma}\rho_0^{\frac{1}{2}} \exp\left(-\frac{1}{2}\beta(y_c + y_a \cos\omega x)\right) \tag{9}$$

Integrated Heat Load with Constant Velocity

To obtain the heat load across a periodic trajectory, Eq. (9) must be integrated over x. To simplify the integration, a small angle approximation for γ is used, and the exponential term is expanded using a Taylor series. Because the maximum flight-path angle for the trajectories discussed in this work remain below 5 deg, a small angle approximation for γ provides better than 0.6% accuracy. Expanding the exponential term leaves the following integral:

$$\int_0^q \mathrm{d}q_{\text{phc}} = \int_0^x C V_0^2 \rho_0^{\frac{1}{2}} e^{-\frac{1}{2}\beta y_c} \times \left[\sum_{n=0}^{\infty} \frac{(-1)^n}{n!}\left(\frac{1}{2}\beta y_a \cos\omega x\right)^n\right] \mathrm{d}x \tag{10}$$

Evaluating the integral from 0 to x leads to

$$q_{\text{phc}} = C V_0^2 \rho_0^{\frac{1}{2}} e^{-\frac{1}{2}\beta y_c}\left(x - \frac{\beta y_a}{2}\frac{\sin\omega x}{\omega} + \frac{(\beta y_a)^2}{8}\left(\frac{x}{2} + \frac{\sin 2\omega x}{4\omega}\right) - \frac{(\beta y_a)^3}{48}\left(\frac{\sin\omega x}{\omega} - \frac{\sin^3\omega x}{3\omega}\right) + \frac{(\beta y_a)^4}{384}\left(\frac{3x}{8} + \frac{\sin 2\omega x}{4\omega} + \frac{\cos 2\omega x}{32\omega} - \frac{1}{32\omega}\right) - \cdots\right) \tag{11}$$

Recall that $\omega = 2\pi/R$; the total heat load presented to a vehicle traveling along a PHC for a single period, from 0 to R, reduces to

$$q_{\text{phc}} = C V_0^2 \rho_0^{\frac{1}{2}} e^{-\frac{1}{2}\beta y_c} R \times \left(1 + \frac{(\beta y_a)^2}{16} + \frac{(\beta y_a)^4}{1024} + \frac{(\beta y_a)^6}{147{,}456}\right) \tag{12}$$

when the first seven terms of the expansion in Eq. (10) are used. The expansion of the exponential term is accurate to within 0.15% for a periodic amplitude of up to 20 km yet provides a relatively compact equation for heat load. Additionally, if the expansion were extended to the first eight terms, the resulting heat load would differ by no more than 0.007% with a periodic amplitude of 20 km.

Periodic Velocity Profile

To achieve greater fuel consumption efficiency compared to a steady-state cruise trajectory, a PHC trajectory relies on the periodic thrusting of the vehicle's engine. Speyer[1,2] has mathematically proven that periodic thrusting is more fuel efficient than continuous thrusting over the same time interval. However, periodic thrusting does not imply that a vehicle flying along a periodic trajectory would maintain a constant velocity. Clearly, drag, lift, and weight would have an affect on the vehicle's velocity, and this must be considered in an attempt to gain a more accurate analytical representation of the heating rates and heat load on the vehicle.

The derivation of the velocity profile of the vehicle is broken into two portions: the glide phase and the skip phase. During the glide phase of the trajectory, the vehicle is influenced by the effects of lift, drag, and weight. Although Eggers and Allen[9] provide a differential equation to estimate the velocity profile of a gliding vehicle with a fixed lift-to-drag ratio, the equation is not easily handled with a changing flight-path angle. Therefore, a slightly different approach is taken to determine the gliding velocity profile. Assuming that the

vehicle's lift balances its weight throughout the gliding portion, the equation of motion that includes drag can be expressed as

$$-\frac{g}{L/D} = \frac{\mathrm{d}V}{\mathrm{d}t} \tag{13}$$

According to work by vE. Rudd et al.,[5] the L/D ratio of a representative hypersonic vehicle flying a PHC trajectory varies by no more than 5% across the trajectory. Therefore, the lift-to-drag ratio is approximated as constant, and Eq. (13) can be solved for position vs time:

$$\frac{\mathrm{d}s}{\mathrm{d}t} = V_0 - \frac{g}{L/D}t \tag{14}$$

where s is the position along the trajectory. Note, however, that the vehicle model developed by Chuang and Morimoto[3] and used by vE. Rudd et al.[5] neglects the change in Reynolds number in calculating the viscous drag. Because the Reynolds number can change by a factor of 20 from the bottom to the top of the PHC trajectories used in this work, the value for the vehicle's viscous drag coefficient at the bottom of a period is roughly a quarter of the value at the top of a period. According to the work of vE. Rudd et al.,[5] if the Reynolds number effects are neglected, the viscous drag accounts for approximately 50% of the vehicle's drag. Therefore, the changing Reynolds number will have some effect on the lift-to-drag ratio of the vehicle as it flies on a PHC trajectory, but those effects were not taken into account in the present work.

To gain a more accurate velocity profile in terms of the horizontal position along the trajectory, the substitution $\mathrm{d}s = \mathrm{d}x \cos\gamma$ is made. Note that γ can readily be written in terms of x. The geometry of the trajectory provides

$$\tan\gamma = \frac{\mathrm{d}y}{\mathrm{d}x} \tag{15}$$

Combining Eq. (15) with the derivative of Eq. (1) with respect to x allows γ to be expressed as

$$\gamma = \arctan(y_a \omega \sin\omega x) \tag{16}$$

By combining the substitution for $\mathrm{d}s$ [Eqs. (16) and (14)], the differential equation becomes

$$\cos[\arctan(y_a \omega \sin\omega x)]\,\mathrm{d}x = \left(V_0 - \frac{-g}{L/D}t\right)\mathrm{d}t \tag{17}$$

By expanding the left-hand side of the differential equation to its first six terms, Eq. (17) can be solved for t:

$$t = \frac{L/D}{g}\left\{V_0 - \frac{1}{420}\sqrt{\left(\frac{g}{L/D}\left(176{,}400V_0^2\frac{L/D}{g} - 352{,}800x + 58{,}800x^3y_a^2\omega^4 - 11{,}760x^5y_a^2\omega^6 - 26{,}460x^5y_a^4\omega^8 + 1120x^7y_a^2\omega^8 + 12{,}600x^7y_a^4\omega^{10} + 15{,}750x^7y_a^6\omega^{12}\right)\right)}\right\} \tag{18}$$

Substituting Eq. (18) into Eq. (14) results in an approximate velocity profile for a vehicle traveling on the gliding portion of a PHC trajectory. The approximation used in Eq. (17) is valid only for the first quarter on either side of the trajectory's starting point. Within this region, using the first six terms provides a high degree of accuracy across a range of y_a and R values, with accuracy increasing as y_a decreases and R increases. With a periodic amplitude of 20 km and a range of 1200 km, the expansion is within 0.2% accuracy and remains within 1% accuracy if either the range is decreased to 800 km or the amplitude is increased to 30 km.

During the skip phase of the trajectory, the flight-path angle increases with time. The effects of weight can be considered negligible in comparison to the lifting force on the vehicle. Thus, the equations of motion simplify to

$$L = mV^2\frac{\mathrm{d}\gamma}{\mathrm{d}x} \tag{19}$$

$$D = -m\frac{\mathrm{d}V}{\mathrm{d}t} \tag{20}$$

Using Eqs. (5) and (15), we can see that for any point along a trajectory

$$\frac{\mathrm{d}y}{\mathrm{d}t} = \frac{\mathrm{d}y}{\mathrm{d}x}\frac{\mathrm{d}x}{\mathrm{d}t} = (\tan\gamma)(V\cos\gamma) \tag{21}$$

Equations (19) and (15) are combined, and the result is combined with Eq. (21) to yield

$$\mathrm{d}t = \frac{mV}{L}\frac{\mathrm{d}\gamma}{\cos\gamma} \tag{22}$$

When Eq. (22) is substituted into Eq. (20),

$$\int_{V_0}^{V}\frac{\mathrm{d}V}{V} = -\frac{C_D}{C_L}\int_{-\gamma_f}^{\gamma}\sec\gamma\,\mathrm{d}\gamma \tag{23}$$

where V_0 and $-\gamma_f$ are the velocity and flight-path angle, respectively, at the beginning of the skipping portion of the trajectory.

The velocity for any point along the skipping segment is then

$$V = V_0\left(\frac{\sec\gamma + \tan\gamma}{\sec(-\gamma_f) + \tan(-\gamma_f)}\right)^{-(C_D/C_L)} \tag{24}$$

where γ is given in terms of position x in Eq. (16).

Because an impulsive ΔV is not realistic, to approximate the increase in velocity during the thrusting portion of the period, it is assumed that one-quarter of the velocity profile undergoes a linear increase in velocity. Effectively, the thrusting would begin when the vehicle is at the lowest point of the trajectory and last until the vehicle reaches the mean altitude of the trajectory. The resulting velocity profile is consistent with the velocity profiles calculated by vE. Rudd et al.[5]

To determine the velocity profile without an impulsive ΔV, a V_{burn} is selected and used as V_0 to determine the velocity profile in the gliding portion of flight, given by Eqs. (14) and (18). Care must be taken in selecting appropriate values for x in Eq. (18) because the gliding portion is physically divided by the definition of the trajectory as a cosine wave. A variation of x from $-0.25R$ to $0.25R$ sufficiently addresses this problem. The velocity at the end of the gliding portion can then serve as V_0 in Eq. (24), and by allowing γ to vary from $-\gamma_f$ to 0, the velocity profile for the first half of the skipping portion can be determined. The velocity profile for the final quarter of the trajectory is approximated as a line drawn from the resulting final velocity to V_{burn}.

To define the magnitude of a velocity profile, a desired average velocity is selected. V_{burn} is then altered until the selected average velocity across the resulting profile is achieved. Figure 2 shows a representative velocity profile for a vehicle averaging 3000 m/s across the trajectory.

Stagnation Heat Flux with Periodic Velocity Profile

Substituting the periodic velocity profile into Eq. (9) and recalling the flight-path angle expression in Eq. (16), we have the heating equation for a PHC trajectory as

$$\frac{\mathrm{d}q_{\text{phc}}}{\mathrm{d}x} = C\frac{V(x)^2\rho_0^{\frac{1}{2}}\exp\left[-\frac{1}{2}\beta(y_c + y_a\cos\omega x)\right]}{\cos[\arctan(-y_a\omega\sin\omega x)]} \tag{25}$$

Heat Load with Periodic Velocity Profile

When the periodic velocity profile is incorporated into Eq. (9), the heat flux equation becomes a complex function of x, and the

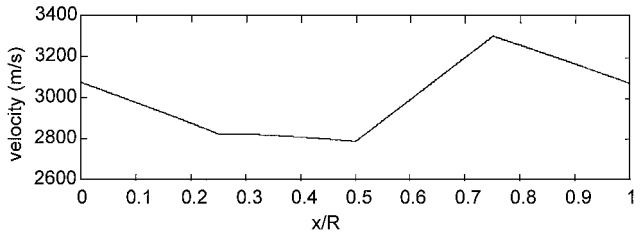

Approximate velocity profile for 3000-m/s average velocity

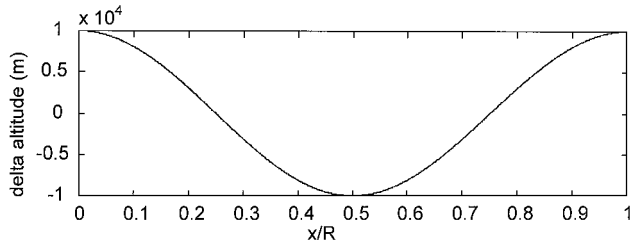

Trajectory profile for 10,000-m amplitude

Fig. 2 Approximate velocity profile for vehicle on PHC trajectory.

integration of the heat flux to obtain the heat load becomes quite involved. It will be seen later that ignoring the velocity profile results in the overestimation of the average stagnation-point heating rates encountered along the trajectory by 1–5%. Therefore, the use of a constant velocity profile provides a conservative approximation of the integrated heat load across the trajectory.

Heating Analysis for Steady-State Cruise

Combining Eq. (6) with the density model of Eq. (7), we can formulate the expression for heat flux along a steady-state cruise trajectory as

$$\frac{\mathrm{d}q_{\mathrm{ss}}}{\mathrm{d}x} = CV_0^2\rho_0^{\frac{1}{2}}e^{-\frac{1}{2}\beta y_{\mathrm{ss}}} \tag{26}$$

The heat load acquired along a steady-state trajectory of distance R then becomes

$$q_{\mathrm{ss}} = CV_0^2\rho_0^{\frac{1}{2}}e^{-\frac{1}{2}\beta y_{\mathrm{ss}}}R$$

Heating Analysis for Hypersonic Glide Trajectory

Hypersonic Glide Velocity Profile

Because the gliding vehicle is assumed to be unpowered, the effects of aerodynamic forces and vehicle weight must be considered when calculating the velocity profile. Eggers and Allen[9] provide a comprehensive analysis of unpowered gliding flight at small flight-path angles, and this analysis is presented in a slightly modified form, beginning with the equations of motion

$$L = -mV_{\mathrm{glide}}^2\frac{\mathrm{d}\gamma_{\mathrm{glide}}}{\mathrm{d}x} + mg - \frac{mV_{\mathrm{glide}}^2}{r_0} \tag{27}$$

$$D = -\frac{1}{2}m\frac{\mathrm{d}V_{\mathrm{glide}}^2}{\mathrm{d}x} + mg\gamma_{\mathrm{glide}} \tag{28}$$

where r_0 is the radius of the Earth or 6370 km.

Dividing Eq. (27) by Eq. (28) provides the differential equation

$$g\left(1 - \frac{L}{D}\gamma_{\mathrm{glide}}\right) + \left(\frac{1}{2}\frac{L}{D}\frac{\mathrm{d}V_{\mathrm{glide}}^2}{\mathrm{d}x} - V_{\mathrm{glide}}^2\frac{\mathrm{d}\gamma_{\mathrm{glide}}}{\mathrm{d}x}\right) = \frac{V_{\mathrm{glide}}^2}{r_0} \tag{29}$$

Because the gliding trajectory is assumed to be a straight path with constant flight-path angle, $\mathrm{d}\gamma/\mathrm{d}x = 0$. Equation (29) then simplifies into a differential equation that can readily be solved for velocity along the gliding trajectory:

$$V_{\mathrm{glide}}^2(x) = \left\{g\left(1 - \frac{C_L}{C_D}\gamma_{\mathrm{glide}}\right) + C_1\left(\frac{1}{r_0}\right)\exp\left(2/r_0\left(\frac{C_L}{C_D}\right)x\right)\right\}\Bigg/\left(\frac{1}{r_0}\right) \tag{30}$$

where

$$C_1 = \left(\left(\frac{1}{r_0}\right)V_{\mathrm{boost}}^2 - g\left(1 - \frac{C_L}{C_D}\gamma_{\mathrm{glide}}\right)\right)\Bigg/\left(\frac{1}{r_0}\right) \tag{31}$$

$$\gamma_{\mathrm{glide}} = \arctan\left(\frac{y_f - y_i}{R_{\mathrm{glide}}}\right) \tag{32}$$

V_{boost} is the velocity of the vehicle at the start of the trajectory. To find the starting velocity, according to Eggers and Allen[9]

$$V_{\mathrm{boost}}^2 = V_s^2\{1 - \exp[-2(R_{\mathrm{glide}}/r_0)/(L/D)]\} \tag{33}$$

where V_s is satellite velocity at the Earth's surface, given as 7903.5 m/s.

Gliding Trajectory Heating Analysis

Combining Eq. (7) with Eq. (2) results in a density profile for the gliding trajectory. With the density profile and the velocity profile given by Eq. (30), the heat flux encountered by a vehicle traveling along a gliding trajectory can be written as

$$\frac{\mathrm{d}q_{\mathrm{glide}}}{\mathrm{d}x} = C\rho_0^{\frac{1}{2}}\exp\left(-\frac{1}{2}\beta\left(\frac{y_f - y_i}{R_{\mathrm{glide}}}x + y_{\mathrm{initial}}\right)\right)\left(\frac{r_0}{\cos\gamma_{\mathrm{glide}}}\right) \times\left\{g\left(1 - \frac{C_L}{C_D}\gamma_{\mathrm{glide}}\right) + C_1\left(\frac{1}{r_0}\right)\exp\left(2/r_0\left(\frac{C_L}{C_D}\right)x\right)\right\} \tag{34}$$

Comparative Heating Analysis

From Eq. (4), it can be seen that the vehicle-specific constant C in Eq. (6) is a weak function of wall temperature and local stagnation temperature. For the purposes of this comparison, the difference between g_w corresponding to a vehicle flying either a PHC, steady-state, or glide trajectory will be considered negligible. Further assuming that all vehicles have the same nose radii, the value of C will be considered the same for all trajectories.

Using the periodic velocity profile derived earlier and retaining γ, we have the ratio of the heating rates acquired along a PHC to the heating rates acquired along a steady-state trajectory reduce to

$$\frac{\mathrm{d}q_{\mathrm{phc}}/\mathrm{d}x}{\mathrm{d}q_{\mathrm{ss}}/\mathrm{d}x} = \frac{V(x)^2\exp\left[-\frac{1}{2}\beta(y_c + y_a\cos\omega x)\right]}{V_{\mathrm{ss}}^2\exp\left(-\frac{1}{2}y_{\mathrm{ss}}\right)\cos[\arctan(-y_a\omega\sin\omega x)]} \tag{35}$$

A similar expression for the ratio of heat flux acquired along a PHC to the heat flux acquired along an unpowered gliding trajectory can be found by dividing Eq. (25) by Eq. (34):

$$\frac{\mathrm{d}q_{\mathrm{phc}}/\mathrm{d}x}{\mathrm{d}q_{\mathrm{glide}}/\mathrm{d}x} = \frac{V(x)^2\exp\left[-\frac{1}{2}\beta(y_c + y_a\cos\omega x)\right]\cos[\arctan(-y_a\omega\sin\omega x)]}{\exp\left(-\frac{1}{2}\beta\{[(y_f - y_i)/R_{\mathrm{glide}}]x + y_{\mathrm{initial}}\}\right)(r_0/\cos\gamma_{\mathrm{glide}})\{g[1 - (C_L/C_D)\gamma_{\mathrm{glide}}] + C_1(1/r_0)\exp[2/r_0(C_L/C_D)x]\}} \tag{36}$$

Results and Discussion

Table 1 summarizes the trajectory parameters used to compare the PHC, steady-state and glide trajectories. The trajectory shapes are shown in Fig. 3 and have the following characteristics.

1) A vehicle flying these trajectories is assumed to have a lift-to-drag ratio of 4 throughout the entire flight, which is consistent with vehicle models used in previous work.[2,4,5]

2) The PHC and steady-state trajectories are designed with a mean Mach number of 10, which is consistent with proposed transatmospheric cruisers[10] and the state of the art in air-breathing propulsion.

3) The glide trajectory is modeled to end at the mean altitude of the steady-state trajectory and minimum altitude of the PHC trajectory.

4) The three trajectories are simulated to achieve a range of approximately half the circumference of the Earth.

Results for the heating analysis can be found in Figs. 4–10. Figure 4 shows the heating rates encountered by a vehicle flying a single PHC period as given by Eq. (25) and a steady-state cruise trajectory as given by Eq. (26). For the PHC trajectory, the highest heating rate is encountered in the center of a period, when the vehicle is at its lowest altitude. The lowest heating rates correspond to the points of highest altitude on the trajectory. Figure 4 also shows that the highest heating rate of the PHC trajectory never reaches the steady-state heating rate. This is because, when both trajectories are at the same altitude, the velocity along the PHC is lower than the steady-state velocity. A comparison of the heating rates encountered along all three trajectories across a distance of 16 PHC periods can be seen in Fig. 5.

Table 1 Trajectory parameters

PHC	SS[a]	Glide
y_c = 40,000 m	y_{ss} = 30,000 m	y_0 = 90,000 m
y_a = 10,000 m	——	y_f = 30,000 m
R = 1,200 km	R = 1,200 km	R_{glide} = 19,200 km
V_{av} = 3,000 m/s	V_{ss} = 3,000 m/s	V_0 = 6,973 m/s
L/D = 4	L/D = 4	L/D = 4

[a]Steady state.

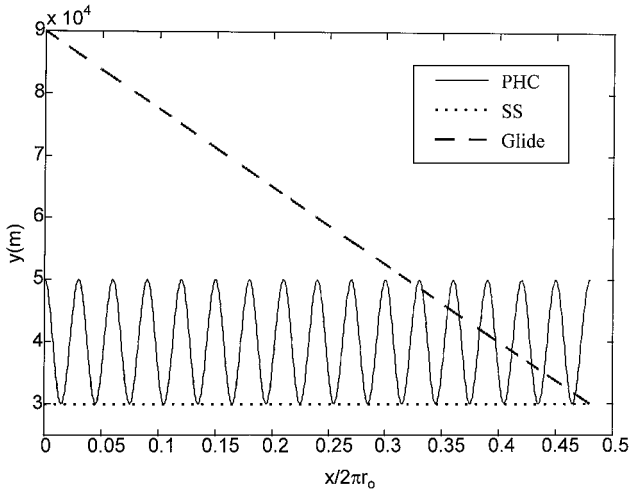

Fig. 3 Comparison of PHC, steady-state (SS), and glide trajectories described in Table 1.

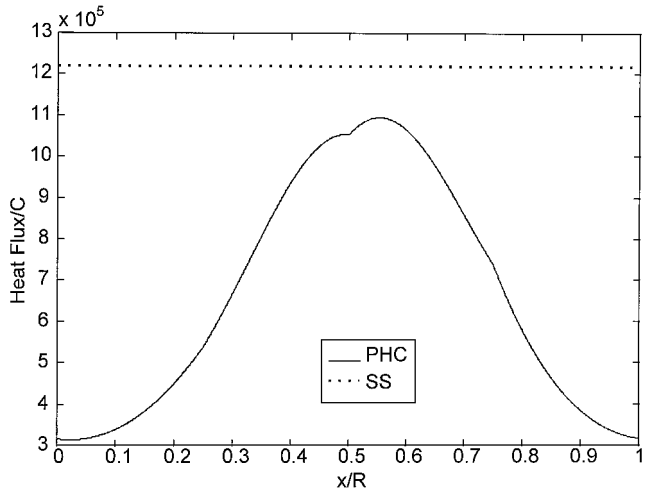

Fig. 4 Comparison of heat flux along PHC and SS trajectories over a single PHC period.

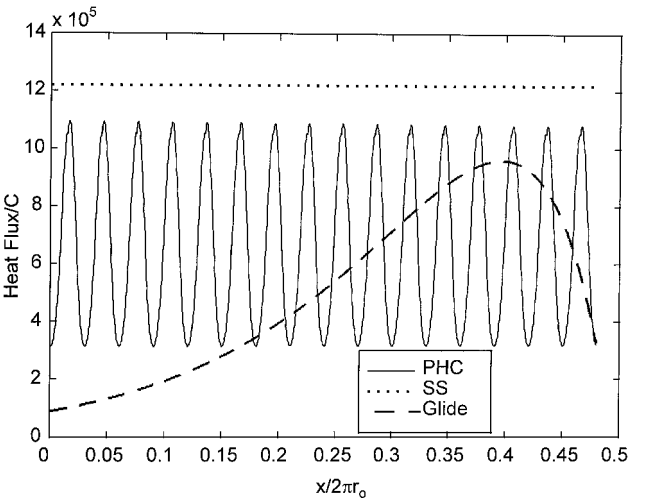

Fig. 5 Comparison of heat flux along PHC, SS, and glide trajectories over 16 PHC periods.

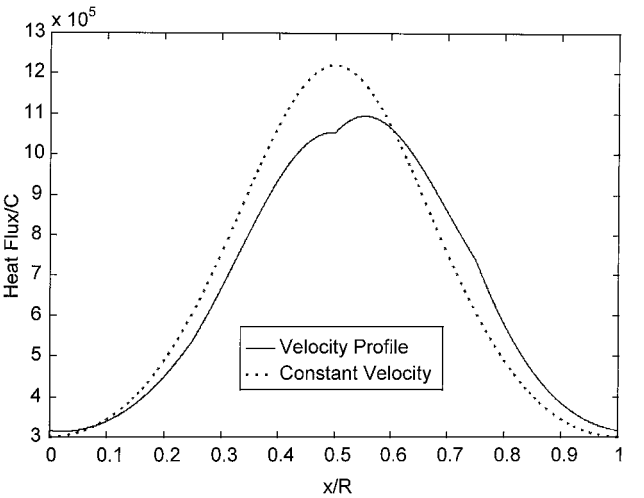

Fig. 6 Comparison of heat flux along a PHC assuming constant velocity and velocity profile.

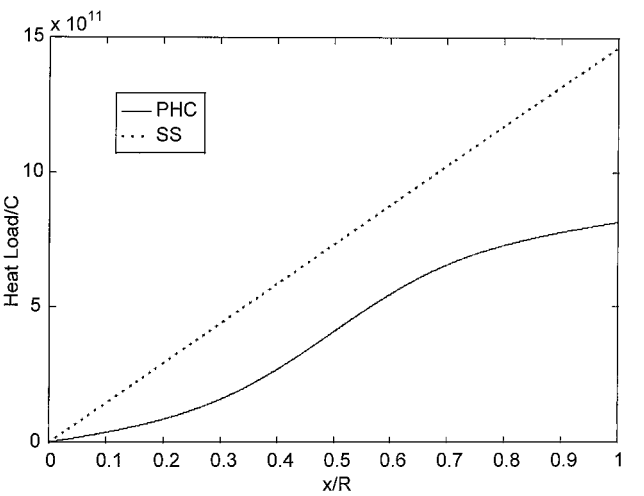

Fig. 7 Comparison of PHC and SS heat loads over a single PHC period.

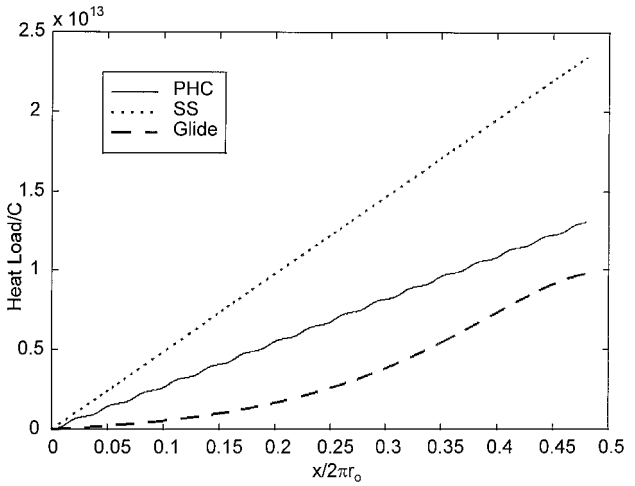

Fig. 8 Comparison of PHC, SS, and glide heat loads over 16 PHC periods.

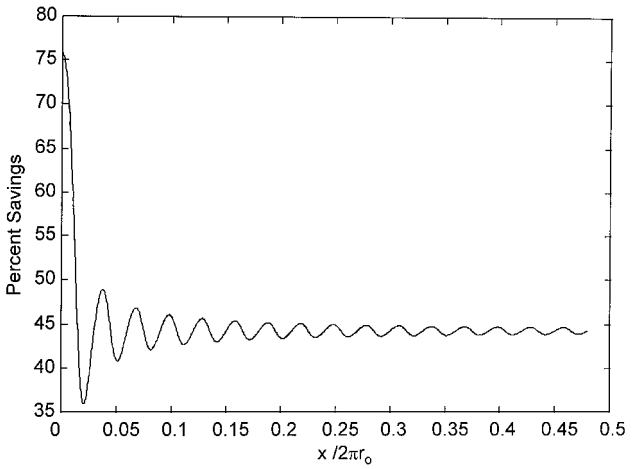

Fig. 9 Percent savings in heat load of PHC over SS across 16 PHC periods.

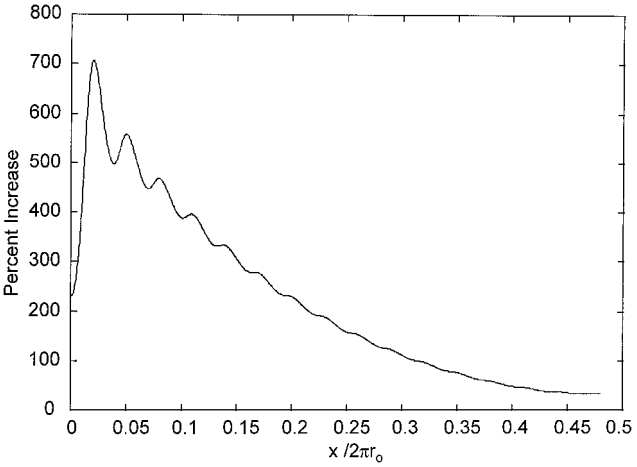

Fig. 10 Percent increase in heat load of PHC over glide across 16 PHC periods.

Figure 6 shows the heat flux encountered by a vehicle traveling on a PHC trajectory with both a constant velocity and the periodic velocity profile. If a vehicle were to fly this trajectory while maintaining a constant velocity, it would encounter only a 2.65% increase in its average heat flux compared to a vehicle traveling with the periodic velocity profile described earlier. Because both cases are examined across the same interval, the ratio of the average heat fluxes is the same as the ratio of the integrated heat flux. This shows that the total integrated heat load is similarly unaffected by the use of a constant velocity across the PHC trajectory. Therefore, it is unnecessary to perform the additional calculations required to find the integral heat load with the periodic velocity profile, inasmuch as the heat load calculated with a constant velocity should suffice for an approximate analysis.

The heat load acquired by a vehicle flying a single period of a PHC trajectory at a constant velocity is shown in Fig. 7. Figure 8 shows the heat load acquired across 16 periods. Figures 7 and 8 also show the heat load obtained along a steady-state trajectory of equal distance, and Fig. 8 shows the heat load from the gliding trajectory. Notice that, for the assumed parameters in Table 1, the heat load presented to a hypersonic vehicle flying a glide trajectory is clearly less than the heat load presented to a vehicle flying a PHC trajectory.

Figure 9 shows the percent savings in heat load over steady state achieved by flying a PHC trajectory. Across the 16 PHC periods shown in Fig. 9, the periodic trajectory accounts for almost a 45% decrease in average heat load compared to the steady-state trajectory. Figure 10 shows the percent increase between the heat load obtained on the PHC trajectory and the glide trajectory. A vehicle flying along the glide trajectory would see a significant reduction in heat load compared to the PHC trajectory throughout most of its flight. When the altitude of the glide path approaches the PHC altitude range, the heat loads begin to approach each other. From Fig. 10, for the case examined, a vehicle flying 16 periods of the PHC trajectory will encounter almost two and a quarter times the heat load absorbed by a vehicle on the glide path of the same distance.

Comparative Results and Analysis

To determine a flight corridor in which PHC trajectories achieve lower average heating rates when compared to the other trajectory types, a comparative analysis was conducted. This analysis includes dynamic pressure constraints on the vehicle, which restrict the vehicle to a dynamic pressure between 24 and 97 kPa. These limits are established by the maximum vehicle structural loads and the operational range of air-breathing propulsion.

Figures 11–14 show the results of the comparative heating rate analysis for a hypersonic vehicle with $L/D = 4$. Figures 11–14 each use either Eq. (35) or Eq. (36) to compare PHC trajectories with amplitudes of 5 and 15 km to a fixed steady-state or glide trajectory. The steady-state trajectory in Figs. 11 and 12 has a mean altitude of 30 km and is flown at a velocity of 3.25 km/s, which is equivalent to a dynamic pressure of 97 kPa. The glide trajectory used in Figs. 13 and 14 is described in Table 1. The PHC trajectories used in the analysis include the velocity profile derived earlier.

The axes of the plots represent varying mean altitudes and average velocities for a PHC trajectory. The contours show the ratio of average PHC heating rates across the trajectory to the average steady-state or glide heating rates. Also shown in Figs. 11–14 is the allowable dynamic pressure corridor for the vehicle. The shaded portions of Figs. 11–14 represent the usable region in which a PHC trajectory can be designed to provide lower average heating rates.

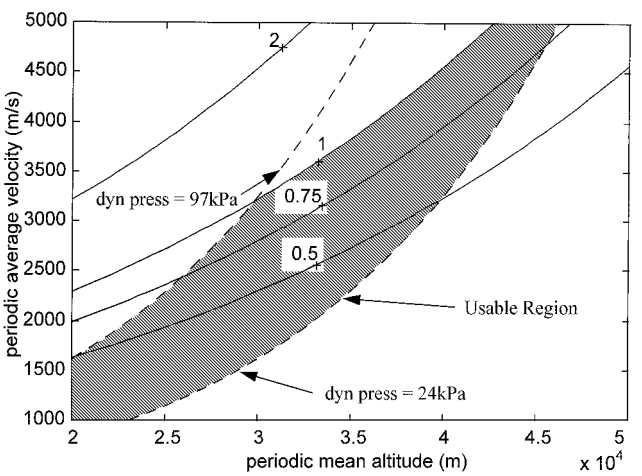

Fig. 11 Ratio of PHC to SS average heating rates (periodic amplitude = 5 km).

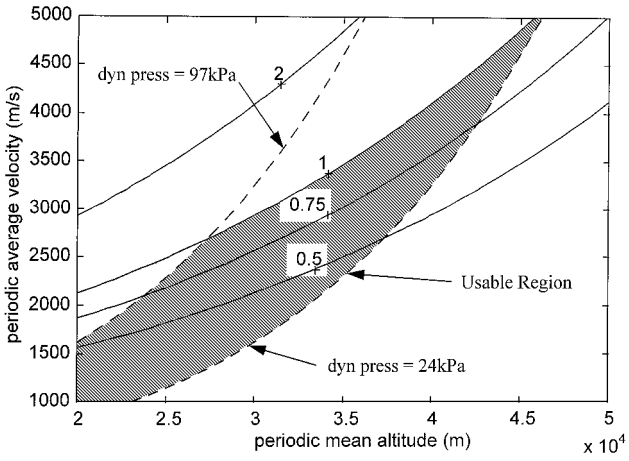

Fig. 12 Ratio of PHC to SS average heating rates (periodic amplitude = 15 km).

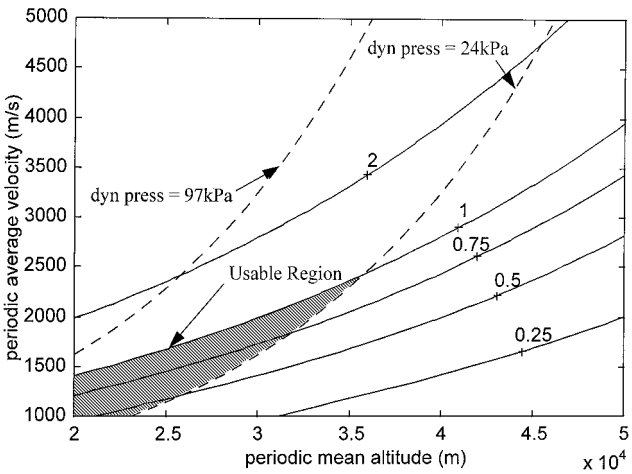

Fig. 13 Ratio of PHC to glide average heating rates (periodic amplitude = 5 km).

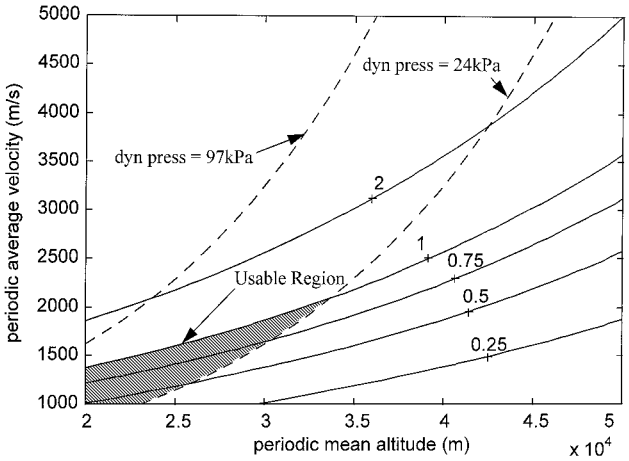

Fig. 14 Ratio of PHC to glide average heating rates (periodic amplitude = 15 km).

From Figs. 11 and 12, it can be seen that, for a PHC trajectory to have a lower average heat flux than a steady-state trajectory, the PHC must be flown either at a lower average velocity or a higher altitude compared to the steady-state path. Figures 13 and 14 show that a PHC trajectory is severely restricted if it is to be designed to result in a lower heating rate than the glide trajectory. The maximum average velocity allowed for the PHC trajectories is barely 2.25 km/s, which is not even half of the average velocity of the glide trajectory in question. Figures 13 and 14 also show that the usable region decreases in size with an increase in periodic amplitude.

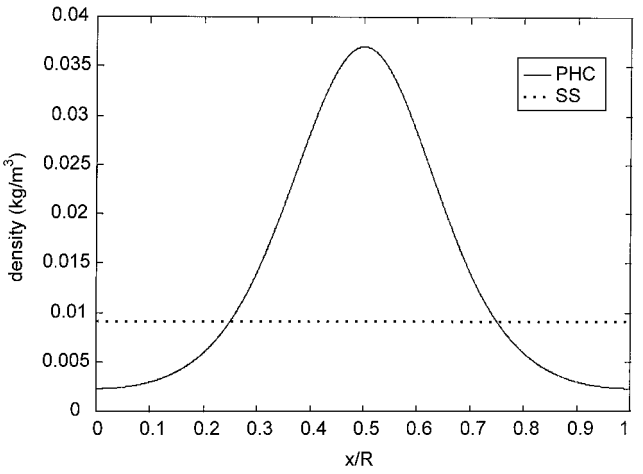

Fig. 15 Density profiles for PHC and SS trajectories.

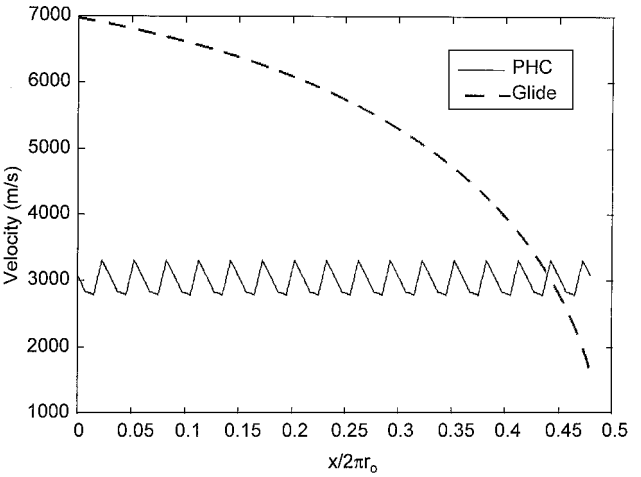

Fig. 16 Velocity profiles for PHC and glide trajectories.

Some insight into the comparative heat flux and resulting heat loads of the steady-state and PHC trajectory types can be found in the density profiles of the trajectories. Figure 15 shows the atmospheric density encountered along a typical periodic trajectory with a 35-km mean altitude and a 10-km amplitude. Overlaid in Fig. 15 is the density at the mean altitude of the trajectory. According to this model, we have the density at the peak of the trajectory dropping by roughly 25% compared to the mean altitude density. However, because the density function varies exponentially, when a vehicle flying along this periodic trajectory reaches its lowest altitude, it encounters an increase in density of almost 400% compared to the mean value. If the same vehicle were to fly a steady-state trajectory at the same average velocity along the mean altitude of the PHC, the vehicle flying the PHC would clearly receive a higher average heat flux across the period. For a PHC trajectory to provide savings in average heating rates and heat loads, it must be either be placed at a higher mean altitude than a comparable steady-state trajectory or the vehicle must travel at a lower average velocity.

The density profile and velocity profiles can also clearly demonstrate why a vehicle traveling on the glide trajectory receives a lower heat load than a vehicle on the PHC trajectory. The mean density encountered along the glide trajectory is only 15% of the mean density through which a vehicle on the PHC trajectory travels, even though almost a third of the glide trajectory is flown within the bounds of the PHC trajectory. At the same time, as the glide trajectory approaches the PHC altitude, the velocity has decreased to the order of the PHC velocities, despite that the glide trajectory being examined has an average velocity almost twice as great as the PHC average velocity. A comparison of the velocity profiles for both trajectory types is shown in Fig. 16. Figure 5 shows that the velocity and density profiles of the glide trajectory combine such that the maximum heating rate of the glide trajectory never exceeds the maximum heat flux of

the PHC trajectory. However, this analysis neglects the boost portion of the trajectory, which would increase the heat load acquired on the gliding trajectory and increase the usable range of PHC trajectory parameters.

Conclusions

This paper has presented a simplified heating analysis for three types of hypersonic cruise trajectories. The approximate analysis supports the conclusion that, for certain combinations of mean altitude, periodic amplitude, and average velocities, vehicles flying PHC trajectories encounter decreased heat loads in comparison to vehicles flying steady-state cruise trajectories. Moreover, the glide trajectories approximated in this work exhibit the lowest heating rates and loads.

The analysis also shows that the reduced heating benefits, attained by flying PHC trajectories, decrease as the periodic amplitude increases. Therefore, heating considerations must be included in PHC trajectory design to obtain a balance between flight performance and heating characteristics for transatmospheric trajectories.

References

[1]Speyer, J. L., "On the Fuel Optimality of Cruise," *Journal of Aircraft*, Vol. 10, No. 12, 1973, pp. 763–765.

[2]Speyer, J. L., "Periodic Optimal Flight," *Journal of Guidance, Control, and Dynamics*, Vol. 19, No. 4, 1996, pp. 745–753.

[3]Chuang, C.-H., and Morimoto, H., "Periodic Optimal Cruise for a Hypersonic Vehicle with Constraints," *Journal of Spacecraft and Rockets*, Vol. 34, No. 2, 1997, pp. 165–171.

[4]Carter, P. H., Pines, D. J., and vE. Rudd, L., "Approximate Performance of Periodic Hypersonic Cruise Trajectories for Global Reach," *Journal of Aircraft*, Vol. 35, No. 6, 1998, pp. 857–867.

[5]vE. Rudd, L., Pines, D. J., and Carter, P. H., "Suboptimal Damped Periodic Cruise Trajectories for Hypersonic Flight," *Journal of Aircraft*, Vol. 36, No. 2, 1999, pp. 405–412.

[6]Allen, H. J., and Eggers, A. J., "A Study of the Motion and Aerodynamic Heating of Ballistic Missiles Entering the Earth's Atmosphere at High Supersonic Speeds," NACA TR 1381, April 1953.

[7]Tauber, M. L., Meness, G. P., and Adelman, H. G., "Aerothermodynamics of Transatmospheric Vehicles," *Journal of Aircraft*, Vol. 8, No. 9, 1987, pp. 594–602.

[8]Nørstrud, H., "On the Integral Heat Load of a Re-Entry Vehicle," AIAA Paper 98-1630, April 1998.

[9]Eggers, A. J., and Allen, H. J., "A Comparative Analysis of the Performance of Long-Range Hypervelocity Vehicles," NACA TR 1382, Dec. 1954.

[10]Takashima, N., Lewis, M. J., and Lockwood, M. K., "Waverider Configuration Development for the Dual Fuel Vehicle," AIAA Paper 96-4593, Nov. 1996.

M. Torres
Associate Editor